Nanoscale

ROYAL SOCIETY OF CHEMISTRY

MINIREVIEW

View Article Online
View Journal | View Issue

Cite this: *Nanoscale*, 2022, **14**, 2155

Self-supported metal–organic framework-based nanostructures as binder-free electrodes for supercapacitors

Xueyan Zhao, Kai Tao * and Lei Han *

Metal–organic frameworks (MOFs), an interesting class of functional inorganic materials, have recently emerged as suitable electrode materials or templates/precursors of electrode materials for supercapacitors (SCs). The key in utilizing MOF-based electrode materials is to address the low electronic conductivity and poor stability issues. Therefore, the rational design and fabrication of self-supported binder-free electrodes is considered the most promising strategy to address these challenges. In this review, we summarize the recent advances in the design and manufacture of self-supported MOF-based nanostructures and their use as binderless electrodes for SCs, especially over the last five years. The synthesis strategies for constructing pristine MOFs, MOF composites and MOF derivative arrays are overviewed. By highlighting the advantages and challenges of each class of electrode materials, we hope that this review will provide some insights into the rational design of MOF-based electrode materials to promote the future development of this highly exciting field.

Received 16th December 2021,
Accepted 13th January 2022

DOI: 10.1039/d1nr08284a

rsc.li/nanoscale

1 Introduction

Global demands for the transmission and storage of renewable energy sources such as solar and wind energy have pushed the development of efficient electrochemical energy conversion and storage technologies including rechargeable batteries, fuel cells and supercapacitors (SCs).[1–9] SCs are promising candidates due to their high power density, rapid charge storage capability, and impressive cycling stability.[10,11] Electrode materials with high capacitance, good rate capability and decent durability are essential for robust and efficient energy storage devices.[12] Rational optimization of nanostructured electrode materials is a promising strategy to maximize the efficiency of SCs.[13–15] Recently, many novel materials have been explored as electrode materials for SCs, and metal–organic frameworks (MOFs) stand out from the rest due to their high specific surface area and potential pseudocapacitance sites.[16–18]

School of Materials Science & Chemical Engineering, Ningbo University, Ningbo, Zhejiang 315211, China. E-mail: taokai@nbu.edu.cn, hanlei@nbu.edu.cn

Xueyan Zhao

Xueyan Zhao was born in 1996, Ningxia Province, China. She is now an M.S. candidate under the supervision of Prof. Kai Tao and Prof. Lei Han at the School of Materials Science and Chemical Engineering, Ningbo University, China. Her thesis focuses on the synthesis of MOF-derived nanostructures and their applications in supercapacitors.

Kai Tao

Dr Kai Tao received his PhD degree from Toyama University (Japan) in 2012 under the supervision of Prof. Noritatsu Tsubaki. Then, he worked in the group of Prof. Liang Chen at the Ningbo Institute of Materials Technology and Engineering, Chinese Academy of Sciences (CAS). Currently, he is a Professor at the School of Materials Science and Chemical Engineering, Ningbo University. His research interest is in the development of porous functional materials for applications in catalysis and energy storage.

MOFs are a kind of porous crystalline material formed by the self-assembly of metal ions/clusters and organic ligands under certain conditions.[19,20] The structure of MOFs can be manipulated by changing the valence states of metal ions and the types of organic ligands. The good crystallinity, large surface area and excellent structural tunability make MOFs the best candidates for high-performance electrode materials.[21] However, the straightforward application of pristine MOFs is impeded by the relatively low electronic conductivity and poor stability during the electrochemical process. Alternatively, MOFs can be transformed into porous carbon, metal oxides/hydroxides, metal sulfides, *etc.*, wherein MOFs are utilized as templates/precursors. MOF derivatives can largely inherit the morphology and high porosity of MOF templates. Therefore, MOFs and MOF-derived electrode materials have attracted increasing attention for application in SCs. Nevertheless, powdery MOF-based electrode materials need to be blended with an insulating polymer binder to form a paste and loaded on a current collector.[22,23] This electrode preparation method suffers from problems such as significant interfacial resistance between the active material and the conductive substrate, forming a "dead volume" and stripping of the active materials, which degrades the advantages of MOF-based electrode materials.[24,25] To overcome these problems, fabricating self-supported MOF-based nanostructures on conductive substrates (nickel foam, carbon cloth, copper foam, *etc.*) without adding binders and conductive additives is a good choice.[26–28] Compared with powdery electrode materials, self-supported binder-free electrodes have the following advantages: (1) direct growth of electroactive materials on conductive substrates simplifies the electrode preparation process. (2) The binder-free electrode ensures rapid electron transfer and good interface contact between the active materials and the substrate. (3) The aligned nanostructures effectively prevent the collapse of electrode materials and expose more electroactive sites.[29–34] In this regard, many MOF-based electrode materials have been directly fabricated on conductive substrates in the forms of self-supported one-dimensional (1D), two-dimensional (2D) and three-dimensional (3D) nanostrucutures in recent years (Scheme 1).[35–38]

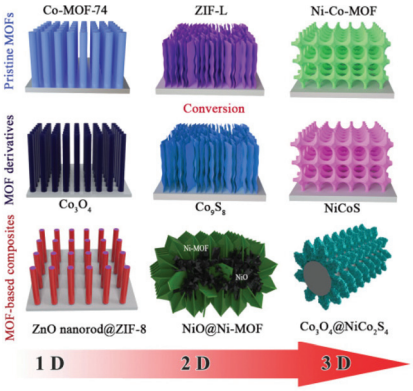

Scheme 1 Schematic illustration of the typical geometry of self-supported MOF-based electrodes for SCs.

A large number of excellent reviews have been published in recent years focusing on MOF-based materials and their applications in energy-related fields.[37] For example, in 2015, Zou and Xu *et al.*[39] gave a critical review on the design principles and strategies for MOFs and MOF-derived nanostructures, and their applications in electrochemical energy storage and conversion. However, powdery MOF-based electrode materials almost dominated the SC applications in these reviews. Given that the integrated electrodes have great promise in SCs, and a growing number of self-supported MOF-based nanostructures have been utilized as binder-free electrodes during the last few years, it is time to give an overview on this topic.

This review will summarize the recent advances in the synthetic strategies of self-supported MOF-based nanostructures, and their utilization as binder-free electrodes for SCs. The challenges faced in this field and the possible solutions to overcome these challenges in order to advance future developments are discussed. Representative works on self-supported MOF-based nanostructures as binder-free electrodes for SCs are listed in Table 1.

2 Self-supported MOF nanostructures

The large specific surface area and inherent redox characteristics make MOFs ideal electrode materials. The bottleneck for the direct use of pristine MOFs in SCs is their low electronic conductivity and poor stability. The electrochemical properties of MOFs can be optimized by preparing self-supported electrodes through the design of multiple morphologies. Besides, coupling with other electrode materials is also an effective strategy to boost the electrochemical performance of MOFs.

Lei Han

Dr Lei Han earned his PhD degree (2005) from the Fujian Institute of Research on the Structure of Matter, Chinese Academy of Sciences (CAS) under the direction of Prof. Maochun Hong. Then, he joined the group of Prof. Pingyun Feng at the University of California – Riverside and the group of Prof. Xiaodong Zou at Stockholm University as a postdoctoral fellow. He is currently a Professor at the School of Materials Science and Chemical Engineering, Ningbo University. His research focuses on the synthesis and application of inorganic–organic hybrid functional materials.

Table 1 Representative self-supported MOF-based nanostructures as binder-free electrodes for SCs

MOF	Electrode	Electrolyte	Capacitance	Capacitance retention	Ref.
Pristine MOF arrays					
Cu–CAT	Cu–CAT NWAs	3 M KCl	202 F g^{-1} at 0.5 A g^{-1}	80% 5000 cycles	40
ZIF-67	TC-ZIF-67	2 M KOH	1.756 F cm^{-2} at 2 mA cm^{-2}	103% 15 000 cycles	44
Co-MOF	Co-MOF nanoplate arrays	2 M KOH	8.56 C cm^{-2} at 5 mA cm^{-2}	84% 5000 cycles	45
Ni/Co-MOF	Ni/Co-MOF@CC	2 M KOH	1180.5 mC cm^{-2} at 3 mA cm^{-2}	97.6% 5000 cycles	50
MOF composite arrays					
Ni-MOF	Co_3O_4@Ni-MOF/NF	1 M KOH	1980.7 F g^{-1} at 1 A g^{-1}	82.2% 2000 cycles	57
Ni-MOF	$NiCo_2O_4$@Ni-MOF/NF	2 M KOH	208.8 mA h g^{-1} at 2 mA cm^{-2}	—	58
ZIF-8	ZnO@ZIF-8/CF	1 M H_2SO_4	390 F g^{-1} at 2 mV s^{-1}	88% 10 000 cycles	64
MOF derivative arrays					
Carbons					
ZIF-67	RPCF/CC	1 M Na_2SO_4	1049 mF cm^{-2} at 12 mA cm^{-2}	98.4% 6000 cycles	70
Co-ZIF	Co–ZIF-450/CC	2 M KOH	1177 mF cm^{-2} at 1 mA cm^{-2}	94% 10 000 cycles	71
Metal oxides					
Co-MOF	Co_3O_4/C NAs/NF	3 M KOH	1.32 F cm^{-2} at 1 mA cm^{-2}	96% 2000 cycles	72
Co–Ni-MOF	2D-CMO/NF	4 M KOH	2098 mF cm^{-2} at 1 mA cm^{-2}	92% 4200 cycles	79
Co-MOF	$ZnCo_2O_4$@NC/CTs	1 M KOH	278.3 mA h g^{-1} at 2 mA cm^{-2}	99.4% 10 000 cycles	80
CoNiMn-MOF	Co_3O_4/NiO/Mn_2O_3/NF	6 M KOH	3652 mF cm^{-2} at 1 mA cm^{-2}	87.6% 10 000 cycles	81
Zn–Co-MOF	ZNCO/rGO/NF	2 M KOH	267 mA h g^{-1} at 1 A g^{-1}	90.2% 6000 cycles	82
Metal sulfides					
Co-ZIF-L	Co_9S_8–NSA/NF	1 M KOH	1098.8 F g^{-1} at 0.5 A g^{-1}	87.4% 1000 cycles	24
Zn/Co-MOF	Zn–Co–S/NF	1 M KOH	2354.3 F g^{-1} at 0.5 A g^{-1}	88.6% 1000 cycles	87
Co-MOF	Fe–Co–S/NF	1 M KOH	2695 F g^{-1} at 1 A g^{-1}	84% 1000 cycles	73
NiCo-MOF	NiCo–S/NF	3 M KOH	3724 F g^{-1} at 1 A g^{-1}	—	88
Zn–Co-ZIF	Ni–Zn–Co–S NSAs/NF	3 M KOH	1.11 mA h cm^{-2} at 10 mA cm^{-2}	85% 1000 cycles	89
Composite arrays derived from MOFs					
Co-MOF	Co_3O_4@$CoNi_2S_4$/CC	2 M KOH	244.4 mA h g^{-1} at 1 A g^{-1}	—	94
Co-MOF-L	Co_3O_4@$NiCo_2O_4$/NF	1 M KOH	544.2 C g^{-1} at 1 A g^{-1}	93% 5000 cycles	95
ZIF-67	LDH@CoS/NF	6 M NaOH	1205 F g^{-1} at 1 A g^{-1}	88.5% 2000 cycles	97
	MMO@Co_3O_4/NF	6 M NaOH	781 F g^{-1} at 1 A g^{-1}	53.7% 2000 cycles	
	Spinelle@C/NF	6 M NaOH	692 F g^{-1} at 1 A g^{-1}	81.9% 2000 cycles	
ZIF-67	Ni–Mo–Co–S NCAs/NF	3 M KOH	1.96 mA h cm^{-2} at 5 mA cm^{-2}	91% 5000 cycles	98
ZIF-67	CC@CoO@S–Co_3O_4	2 M KOH	1013 mF cm^{-2} at 1 mA cm^{-2}	67.7% 5000 cycles	99
ZIF-67	$Zn_{0.76}Co_{0.24}S$ CSNSAs	3 M KOH	1202 C g^{-1} at 1 A g^{-1}	92% 5000 cycles	100

2.1 Synthesis of pristine MOF arrays

2.1.1 ***In situ* growth.** The *in situ* growth of MOF nanostructures on conductive substrates is the straightforward approach to prepare self-supported binder-free electrodes. In a typical process, conductive substrates such as nickel foam (NF), carbon paper (CP) and carbon cloth (CC) are added into the synthesis solution of MOFs, and the nucleation and growth of MOF nanocrystals on the substrates occur. MOFs with various geometric morphologies can be obtained by choosing appropriate metal nodes, organic linkers and synthesis conditions. As a typical example, Li *et al.* reported conductive Cu–CAT nanowire arrays (NWAs) grown directly on carbon fiber paper (CFP) by invading the CFP into a reaction solution containing copper acetate monohydrate and 2,3,6,7,10,11-hexahydroxytriphenylene (HHTP).[40] Cu ions coordinated with HHTP ligands in the *ab* plane to construct a 2D hexagonal lattice, which further packed along the *c*-axis with a slipped-parallel AB stacking model to form a honeycomb-like porous structure (Fig. 1a). Cu–CAT had 1D channels along the *c*-axis with an open-window size of ≈1.8 nm. As shown in the scanning electron microscopy (SEM) images in Fig. 1b and c, a large number of densely oriented nanowires uniformly covered the entire fiber. The 1D channels in the Cu–CAT crystal structure extended along the growth direction of the nanowires,

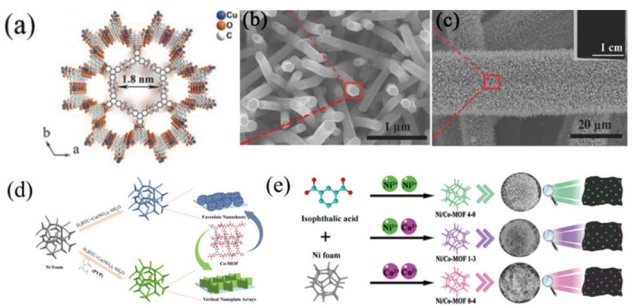

Fig. 1 (a) Crystal structure of Cu–CAT viewed along the *c*-axis and (b and c) SEM images of Cu–CAT NWAs growing on carbon fiber paper. Reprinted with permission from ref. 40, Copyright 2017, Wiley-VCH. (d) Schematic illustration of the synthesis of faveolate Co-MOF nanosheets and Co-MOF nanoplate arrays. Reprinted with permission from ref. 45, Copyright 2021, Elsevier. (e) Schematic diagram of the synthesis process of Ni/Co-MOF with different molar ratios of Co/Ni. Reprinted with permission from ref. 49, Copyright 2021, Royal Society of Chemistry.

facilitating the electrolyte ion transport. The Cu–CAT NWAs showed excellent electrochemical performance as a binder-free electrode for SCs. The specific capacitance of Cu–CAT NWAs was 202 F g^{-1} at 0.5 A g^{-1}, which was twice that of the powder electrode. When the current density was increased from 0.5 to

10 A g^{-1}, Cu–CAT NWAs displayed a high rate performance (66% retention). Besides, 80% of their initial capacitance was retained after 5000 cycles, and no change in the crystalline structure of spent Cu–CAT NWAs was found, indicating their good electrochemical stability.

Recently, 2D materials have emerged as ideal electrode materials for SCs. The atomic thicknesses with short paths and large lateral dimensions of 2D materials allow fast mass transport and superior electron transfer.[12,41–43] Due to the synergistic advantages of 2D nanostructures, MOFs and self-supported configurations, 2D MOF nanoarrays, including nanosheets and nanowalls, have attracted extensive attention. Cobalt-based MOFs represent important MOF materials that have shown promising applications in electrochemical energy storage. In this context, Ma *et al.* reported the *in situ* growth of cobalt-based zeolitic imidazolate framework-67 (Co-ZIF-67) flakes on textile carbon cloth (TC) by a simple immersing method.[44] TC was composed of helical carbon fibers with many wrinkles. These wrinkles increased the adsorption of Co ions on TC, thus facilitating the nucleation and growth of ZIF-67 nanocystals on the TC substrate. TC-ZIF-67 showed extremely improved conductivity compared with ZIF-67. As a free-standing electrode for SCs, TC-ZIF-67 displayed an areal capacitance of 1.756 F cm^{-2}. More importantly, the electrode exhibited outstanding cycling stability. About 103% of the initial capacitance was retained even after 15 000 cycles at a current density of 40 mA cm^{-2}. Similarly, Zhang and co-workers used polyvinylpyrrolidone (PVP) as a regulator to prepare vertical Co-MOF nanoplate arrays on NF, while faveolate nanosheets were obtained without adding PVP (Fig. 1d).[45] When utilized as binder-free electrodes for SCs, both electrodes with different morphologies showed excellent electrochemical performance. Particularly, the vertical Co-MOF nanoplate arrays delivered a much higher areal capacity (8.56 C cm^{-2}) at a current density of 5 mA cm^{-2} compared with faveolate Co-MOF nanosheets (2.4 C cm^{-2}). This was explained by the fact that the vertical nanoplate array structure was much more beneficial for the ion transport and infiltration of electrolytes. Nickel-based MOFs are also widely explored as electrode materials for SCs due to their high electrochemical activity. For example, Yang *et al.* reported a layered 2D Ni-MOF grown directly on NF, which exhibited a high specific capacitance due to the layered structure and favourable exposed facets.[46] Bimetallic MOFs with multiple valence states and improved electronic conductivity were more appealing as electrode materials for SCs than single-metal MOFs.[47] Wang *et al.* fabricated a triangular array of bimetallic Ni–Co MOF nanosheets on NF by one-step hydrothermal synthesis.[48] The tight connection between the aligned MOF arrays and NF ensured a fast charge transfer. Interestingly, by adjusting the molar ratio of Ni to Co, NiCo-MOF/NF with a Ni/Co ratio of 3 : 2 showed the best electrochemical performance. The optimal NiCo-MOF/NF could provide a high specific capacitance of 2230 F g^{-1} at 1 A g^{-1}, and a hybrid SC made with NiCo-MOF/NF and activated carbon (AC) could provide excellent energy density (34.3 W h kg^{-1}) at a power density of 375 W kg^{-1}. The construction of bimetallic MOF nanoarrays on conductive substrates could significantly improve the electrochemical performance of MOF electrode materials in SCs.

Compared with low-dimensional nanostructures, 3D nanostructures have larger accessible surface areas and interconnected networks, which are conducive to redox reactions. Therefore, various 3D MOF nanostructures, such as flowers and honeycombs, have been integrated with conductive substrates. As a typical example of self-supported 3D MOF electrodes, Chen *et al.*[50] fabricated a porous Ni/Co based MOF with a honeycomb structure directly on carbon cloth (Ni/Co-MOF@CC) though a hydrothermal method using $H_{32}Mo_7N_6O_{28}$ as a catalyst. The good electrical conductivity and the porous wasp-like structure endowed the Ni/Co-MOF@CC electrode with good electrochemical properties. The prepared Ni/Co-MOF@CC electrode exhibited a high specific capacitance of 1180.5 mC cm^{-2} at 3 mA cm^{-2} and good rate performance (624.1 mC cm^{-2} at 60 mA cm^{-2}). In addition to designing MOFs into a honeycomb structure, Ren and co-workers prepared a series of flower-like bimetallic Ni/Co-MOFs on NF using a simple solvothermal synthesis method (Fig. 1e).[49] The composition and morphology of the flower-like bimetallic Ni/Co-MOFs can be adjusted by changing the Ni/Co ratio (molar) of the synthesis solution. As a binder-free SC electrode, the optimal sample displayed an excellent specific capacitance of 1230.3 F g^{-1} at a current density of 1 A g^{-1}. The assembled solid-state asymmetric supercapacitor (ASC) using the optimal sample as the positive electrode and AC as the negative electrode exhibited an ultra-high energy density of 116 W h kg^{-1} at a power density of 0.79 kW kg^{-1} and a superior stability with 92.1% initial capacitance retention even after 6000 cycles at 10 A g^{-1}.

The above results indicate that the drawbacks (*i.e.* poor electrical conductivity and structural instability) of pristine MOFs can partially be overcome by designing them into on self-supported 1D, 2D and 3D nanostructures on conductive substrates, and the *in situ* growth method provides a straightforward strategy to fabricate such nanostructures. It should be noted that careful control of the synthesis parameter is needed to obtain the desirable morphology and compositions.

2.1.2 Template strategy. Although the *in situ* growth method is simple, this strategy can only succeed in limited cases. The direct fabrication of MOF arrays remains challenging due to the low heterogeneous nucleation density of most MOF crystals on conductive substrates. Besides, the MOF nanocystals are usually randomly orientated. To overcome the above-mentioned drawbacks, a template strategy for constructing MOF arrays on conductive substrates is developed, which is regarded as one of the most effective methods to improve the conductivity and shape orientation of MOFs. Metal oxides/hydroxides with a vertical orientation and a large specific surface area can be utilized as promising templates and precursors. After reaction with organic linkers, self-supported MOF nanostructures are obtained by pseudomorphic transformation. For example, Deng *et al.* used $Co(OH)_2$ as a precur-

sor or template to prepare oriented MOF arrays on carbon fiber paper (CFP), and the synthesis process was analogous to the RNA reverse transcription (Fig. 2a).[51] First, vertically oriented $Co(OH)_2$ was electrodeposited on CFP as a template and precursor, and then nickel ions and terephthalic acid (PTA) were added. The nickel ions replaced the H atoms on the $Co(OH)_2$ layer as anchoring sites for further self-assembly of the MOF, and a vertically-oriented CoNi-MOF array was grown on CFP (Fig. 2b and c). The $Co(OH)_2$-derived oriented MOF array exhibited very promising electrochemical performance compared to the powdery MOF electrode. The specific capacitance of Co–Ni-MOF/CFP electrodes was as high as 1044 F g^{-1} at 2 A g^{-1}. The assembled ASC device was able to provide a maximum energy density of 28.5 W h kg^{-1}. In another work, Zhang *et al.* proposed an effective strategy to improve the electrical conductivity and electrochemical properties of MOFs by employing $Ni(OH)_2$ electrochemically deposited on carbon nanowalls as the precursor and template for preparing aligned Ni-MOFs.[52] The as-synthesized vertically oriented MOF flakes displayed a specific capacitance of 677 F g^{-1} at a current density of 2 A g^{-1}, which was almost three times that of the MOF powder (239 F g^{-1}). The corresponding ASC device delivered a maximum energy density of 20.7 W h kg^{-1} and a maximum power density of 23 200 W kg^{-1}. Xu *et al.* prepared a layered-structure CoNi-MOF with ultrathin nanosheets and nanotube arrays directly on CC using $Co(OH)_2$ as the template and Co source (Fig. 2d).[53] The synthesized CC/CoNi-MOF showed a high areal capacity (1.0 C cm^{-2}) at 2 mA cm^{-2} and good rate capability (61.4% retention at 15 mA cm^{-2}). A hybrid SC was successfully fabricated with CC/CoNi-MOF as a positive electrode and reduced graphene oxide–carbon nanotubes as a negative electrode, and it delivered a maximum areal capacitance of 846 mF cm^{-2} at 1 m A cm^{-2} corresponding to a high energy density of 55.5 W h kg^{-1} at 175.5 W kg^{-1}, and excellent cycling stability (96.5% after 10 000 cycles).

The above results show that the template strategy is an effective way to construct MOF arrays on conductive substrates. The metal oxide/hydroxide template guides the oriented growth of MOF crystals and is also acted as a metal ion source for MOF growth.[54] This greatly optimizes the connection of the active materials to the substrate, giving rise to improved mechanic stability and electronic conductivity. This strategy provides a universal protocol for designing self-supported MOF nanostructures by choosing proper templates and organic linkers. However, the crystal size and shape of the MOF structures depend strongly on the physicochemical properties of the template and the synthesis parameters. Therefore, precise control of the synthesis parameters is required.

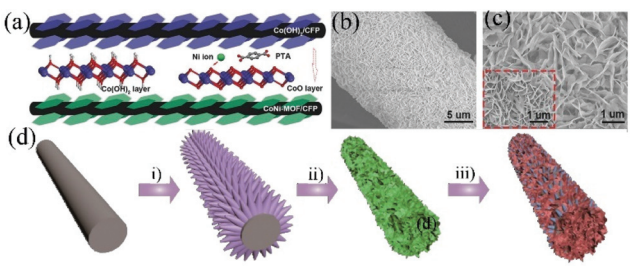

Fig. 2 (a) The schematic illustration of the synthesis of CoNi-MOF, and the SEM images of (b) the $Co(OH)_2$ precursor and (c) CoNi-MOF. Reprinted with permission from ref. 51, Copyright 2017, Wiley-VCH. (d) Schematic illustration of the preparation of CC/CoNi-MOF. (i) Formation of ZnO nanoarrays, (ii) deposition of $Co(OH)_2$ nanosheets and (iii) transformation of $Co(OH)_2$ to CoNi-MOF. Reprinted with permission from ref. 53, Copyright 2020, Elsevier.

As electrodes, MOF arrays are advantageous to MOF powders since non-conductive binders and conductive additives are avoided. Besides, the orientated nanocystals are beneficial for the electrode kinetics. However, the electrochemical performance of single MOFs is still limited.

2.2 Synthesis of MOF composite arrays

To overcome the intrinsic low electronic conductivity and instability of pristine MOFs, it is commonly combined with conductive materials (*e.g.*, carbon nanotubes, graphene, and conductive polymers) to form a MOF composite, which exhibits improved electrochemical properties. However, the aggregation of MOF particles is unavoidable, and the porous structure of the MOF is blocked to some extent. Besides, the powdery MOF composite is needed to be mixed with conductive additives and polymer binders to prepare the electrode, resulting in a low utilization of active sites and a large electrical resistance, which deteriorates the electrochemical performance of the MOF composite. Thus, it is desirable to integrate MOFs with an array of secondary electrode materials to form MOF composite arrays as binder-free electrodes for SCs. In this circumstance, transition metal oxides (TMOs) are ideal scaffolds for anchoring MOFs since they can be designed into various nanoarrays through a simple hydrothermal synthesis or electrodeposition. Therefore, this section will focus on the hybridization of TMOs with MOFs on conductive substrates to form free-standing electrodes for SCs.[10,55,56]

2.2.1 Growth of MOFs on TMO arrays. TMOs typically have multiple oxidation states and structures capable of rich redox reactions. Thus, the hybridization of MOFs with self-supported TMO nanoarrays can significantly improve the specific capacitance of MOFs. In addition, the oriented MOFs can mitigate the small specific surface area and agglomeration tendency of TMOs. In this regard, Bi *et al.* prepared hierarchical Co_3O_4@Ni-MOF nanosheet hybrid arrays on NF by immobilizing ultrathin Ni-MOF nanosheets on self-supported Co_3O_4 nanoarrays through a solvothermal method (Fig. 3a).[57] The Ni-MOF nanosheets (only a few tens of nanometers) were vertically aligned on the surface of the Co_3O_4 nanosheets (Fig. 3b and c). Such a core–shell nanosheet structure could take full advantages of each component. Thus, the obtained Co_3O_4@Ni-MOF electrode exhibited a specific capacitance as high as 1980.7 F g^{-1} at 1 A g^{-1}. The asymmetric two-electrode cell assembled with AC also provided excellent energy density.

Compared with monometallic oxides, mixed-metal TMOs possess higher conductivity and undergo richer redox reactions. As a result, spinel MCo_2O_4 (M = Zn and Ni) is more

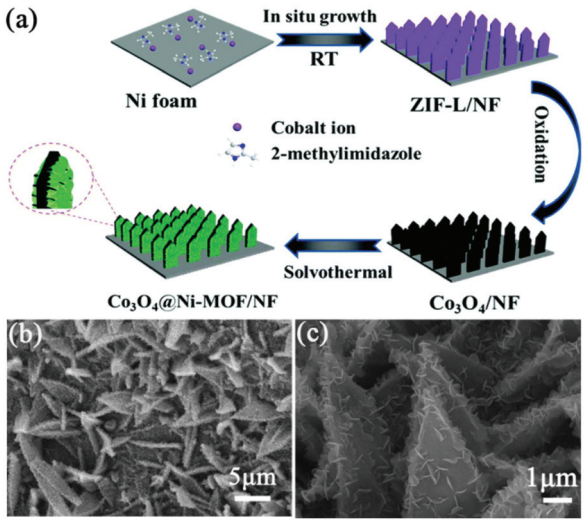

Fig. 3 (a) Schematic illustration of the preparation of Co_3O_4@Ni-MOF/NF. (b and c) SEM images of the as-prepared Co_3O_4@Ni-MOF/NF. Reprinted with permission from ref. 57, Copyright 2021, Royal Society of Chemistry.

appealing as electrode material. Li *et al.* prepared a $NiCo_2O_4$ nanowire array on carbon fiber (CF) by a simple two-step method, which was utilized as a scaffold for anchoring MOF crystals (Fig. 4a).[58] The growth of Ni-MOF nanosheets on the surface of $NiCo_2O_4$ nanowires was modulated by the reaction time and the concentration of the synthesis solution. The quantity of Ni-MOF shells was progressively increased with the increase of reaction time from 3 to 24 h (Fig. 4b–e) and the concentration of the synthesis solution. The optimized $NiCo_2O_4$@Ni-MOF composite array electrode showed excellent specific capacity (208.8 mA h g^{-1} at 2 mA cm^{-2}). Furthermore, the assembled $NiCo_2O_4$@Ni-MOF//AC ASC device exhibited a maximum energy density of 32.6 W h kg^{-1} at a power density of 348.9 W kg^{-1}. Notably, $NiCo_2O_4$@Ni-MOF displayed excellent cycling durability benefiting from the robust core–shell structure and binder-free feature, maintaining 100% incipient capacitance after 6000 cycles at a current density of 8 mA cm^{-2}. In addition to $NiCo_2O_4$, nanoarrays of binary metal oxides such as $ZnCo_2O_4$, $MnCo_2O_4$ and $CuCo_2O_4$ on conductive substrates can be used scaffolds for the deposition of MOFs.[59,60]

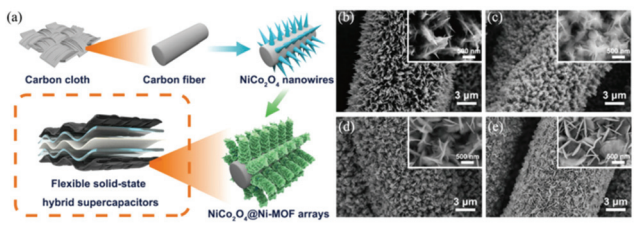

Fig. 4 (a) Schematic illustration of the synthesis of $NiCo_2O_4$@Ni-MOF on CF. (b–e) SEM images of $NiCo_2O_4$@Ni-MOF synthesized at 3, 6, 12, and 24 h for MOF growth, respectively. Reprinted with permission from ref. 58, Copyright 2019, American Chemical Society.

2.2.2 Partial conversion of TMO arrays. TMO arrays grown on conductive substrates have received much attention in recent years as templates/precursors for preparing TMO/MOF composites in the field of electrochemical energy storage. The combination of MOFs and TMOs can benefit from the advantages of both, while avoiding their disadvantages. More importantly, the partial conversion of TMOs to MOFs gives rise to TMO/MOF heterostructures, which facilitates the charge transfer. Recently, ZnO nanowire electrodes have attracted a lot of attention since they can be simply synthesized by hydrothermal synthesis. 1D ZnO nanowires have proven to be good scaffolds for supporting secondary electroactive materials due to their relatively good conductivity and large specific surface area. Interestingly, ZnO could provide Zn^{2+} as the metal ion source for the synthesis of ZIF-8.[61,62] For example, ZnO and cobalt carbonate hydroxide nanowires were grown on conductive CC by the hydrothermal method, and the nanowire samples were exposed to 2-methylimidazole (2-MIM) vapor to form ZnO@ZIF-8 and $Co(CO_3)_{0.5}(OH)\cdot 0.11H_2O$@ZIF-67 nanowires (Fig. 5a).[63] The evaporated 2-MIM reacted with the metal ions on the nanowire surface and continuously transformed the metal oxides/hydroxides into MOFs. The rooting of the metal oxides on the substrate effectively inhibited mechanical shedding and greatly optimized the attachment of the active materials to the substrate. The MOF particles anchored on the surface of the 1D nanostructure overcame the problem of aggregation between the particles and collapse of the structure. Such hybrid MOF arrays were promising electrode materials for SCs. In another work, Liu *et al.* soaked a ZnO nanorod/cotton composite fabric into a DMF solution contain-

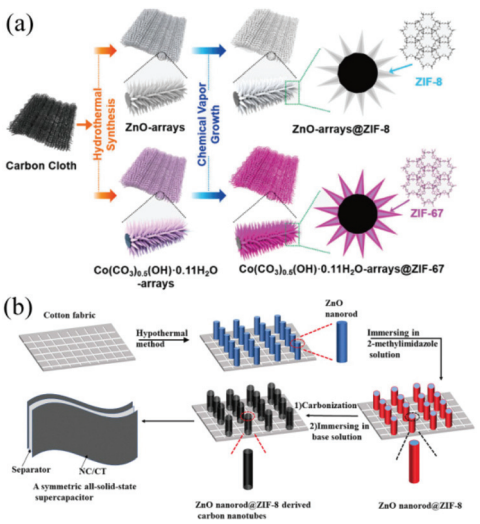

Fig. 5 (a) Scheme showing the synthetic process of ZnO@ZIF-8 and Co $(CO_3)_{0.5}(OH)\cdot 0.11H_2O$@ZIF-67 on CC. Reprinted with permission from ref. 63, Copyright 2018, American Chemical Society. (b) Schematic illustration showing the fabrication of ZnO@ZIF-8 derived nanotubes. Reprinted with permission from ref. 64, Copyright 2018, Elsevier.

ing 2-MIM, and the ZnO nanorods slowly dissolved and the released Zn^{2+} ions reacted with 2-MIM to form a layer of ZIF-8 on the surface of ZnO nanorods, and the space between the ZnO nanorods was not blocked by the ZIF-8 shell layer (Fig. 5b).[64] The core–shell ZnO@ZIF-8 nanorod array was carbonized, and the final carbon electrode exhibited excellent electrochemical performance (390 F g^{-1} at 2 mV s^{-1}). The assembled all-solid-state ASC device delivered a high energy density of 23.4 W h kg^{-1} at a power density of 91.4 W kg^{-1}.

The above studies show that self-supported TMO/MOF hybrid arrays can be constructed by the growth of MOFs on TMO or partial transformation of TMOs into MOFs, and the combination of MOFs with TMOs is an effective way to further improve the energy storage performance of MOF-based electrodes. However, there are many fundamental and technical challenges to be overcome before MOF composites can meet the requirements of SC devices. A better understanding of the MOF composite mounting mechanism is highly desirable to guide and explore the incorporation of other electrode materials such as carbon, conductive polymers and metal sulfides with MOFs to form hybrid arrays.

3 Self-supported nano-structures derived from MOF templates

Apart from being directly used as electrode materials, MOFs have recently been extensively explored as a promising template/precursor for constructing electrode materials. The thermal transformation of MOFs yields a variety of nanostructured materials, including porous carbon, metal oxides and metal sulfides. These MOF derivatives are characterized by a high specific surface area, permanent pores and controlled functionality, which make them suitable as electrode materials. This section will give an overview on recent advances in self-supported nanostructures derived from MOF templates, and the use of them in SCs.

3.1 Direct conversion of MOF nanostructures

3.1.1 MOF-derived porous carbons. Nanoporous carbon materials have attracted much attention in SCs because of their large specific surface area, good electrical conductivity and excellent chemical stability. Due to their high carbon content, MOFs can be used as precursors to prepare carbon materials without requiring the use of a secondary carbon source. Since the pioneering work of Xu's group,[65] many nanoporous carbons have been successfully prepared by direct carbonization of various MOF precursors, such as MOF-5, ZIF-8, ZIF-67 and MIL-88.[66–68] For example, a flexible porous carbon film composed of porous carbon polyhedra and carbon nanotubes (CNTs) derived from MOFs was firstly reported as a binder-free SC electrode by Liu *et al.*[69] Due to the synergistic effect of carbon polyhedra and CNTs, the carbon electrode showed a high specific capacitance of 381.2 F g^{-1} at 5 mV s^{-1} and a good cycling stability with a coulombic efficiency of more than 95% after 10 000 cycles at 10 A g^{-1}. This work provided a new way to design MOF-based porous carbon films as binder-free electrodes for high-performance energy storage devices. Zhang *et al.* prepared a hydrophilic, porous and heteroatom-doped carbon foam by annealing the ZIF-67 precursor followed by surface modification.[70] An array of triangular ZIF-67 with an average thickness of 120 nm was first grown on CC (Fig. 6a). ZIF-67 contains a high carbon content and can be directly converted to a carbon–metal porous material without secondary carbon precursors. After calcination under an inert atmosphere, 3D graphitic foam-like carbon was formed with a large number of visible macropores (10–30 nm), as shown in Fig. 6b. The optimized CC supported porous carbon foam (RPCF/CC) exhibited a maximum capacitance of 1.049 F cm^{-2} at a current density of 12 mA cm^{-2} and a capacitance retention of 98.4% after 6000 charge/discharge cycles at 15 mA cm^{-2}. The ASC device assembled by coupling the carbon foam with an MnO_2/CC cathode in a neutral Na_2SO_4 aqueous electrolyte could provide an energy density of up to 10.1 mW h cm^{-3}. A similar work was performed by Song *et al.*, who synthesized a Co-MOF nanocuboid on CC, and then transformed the Co-MOF into nanoporous N-doped carbon nanocubes encapsulated with cobalt oxide and Co metal (Co-ZIF-450/CC) by annealing the Co-MOF under an N_2 atmosphere (Fig. 6c).[71] The highly conductive Co metal and N-doped carbon networks facilitated the electron transport. The nanopores acted as a reservoir for the electrolyte, reducing the diffusion distance of ions from the electrolyte to the electrode surface. Benefiting from these factors, the prepared electrode displayed a high areal capacitance (1.177 F cm^{-2} at 1 mA

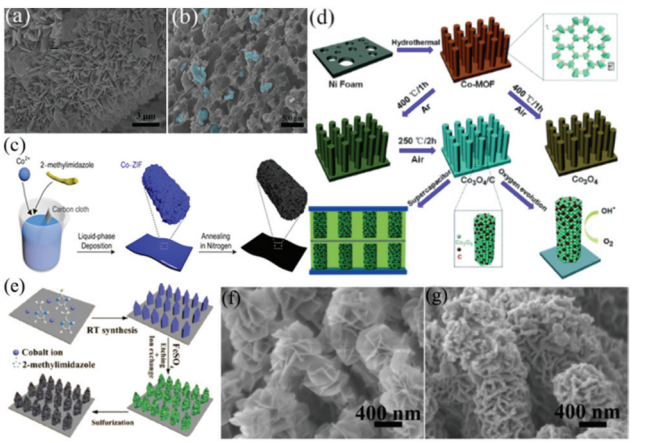

Fig. 6 SEM images of (a) ZIF-67/CC and its derived (b) carbon foam. Reprinted with permission from ref. 70, Copyright 2019, Elsevier. (c) Schematic illustrating the synthesis of a cobalt-containing nanoporous N-doped carbon nanocuboid. Reprinted with permission from ref. 71, Copyright 2019, MDPI. (d) Schematic illustration of the synthesis of hybrid Co_3O_4/C electrodes for application in SCs and the oxygen evolution reaction. Reprinted with permission from ref. 72, Copyright 2016, Royal Society of Chemistry. (e) Schematic illustration of the fabrication of Fe–Co–S/NF, and the SEM images of (f) LDH@Co-MOF/NF and (g) Fe–Co–S/NF. Reprinted with permission from ref. 73, Copyright 2019, Elsevier.

cm^{-2}) and outstanding cycling stability (94% capacitance retention after 20 000 cycles).

3.1.2 MOF-derived metal oxides. In comparison to carbon materials storing charge through electrostatic accumulation of charges, usually known as electric double-layer capacitors (EDLCs), metal oxides display much higher specific capacitance arising from near-surface faradaic redox reactions. In recent years, the template method has been widely adopted to synthesize metal oxides with particular size and shape. MOFs possess tunable structures and high porosity, thus they can be utilized as effective templates to construct porous metal oxide nanostructures with highly customizable compositions, structures and properties.[55,56,74–76] Co_3O_4 is an attractive electrode material for SCs due to its extremely high theoretical capacitance (3650 F g^{-1}). However, its slow redox reaction kinetics and low electronic conductivity result in unsatisfactory electrochemical performance in practice.[77] To solve this problem, constructing porous metal oxide nanostructures supported on conductive substrates is considered as a key strategy to improve the energy storage performance. For example, porous Co_3O_4/C nanowire arrays (NAs) were fabricated on NF by thermally annealing Co-MOF in argon and air, respectively, as shown in Fig. 6d.[72] The porous Co_3O_4/C NAs/NF as a SC electrode showed a good specific capacitance of 1.32 F cm^{-2} at 1 mA cm^{-2}, which was much higher than that of Co_3O_4. The enhanced electrochemical performance was ascribed to the good conductivity of binder-free interconnected carbon networks and the MOF-derived hierarchical porous structure facilitating ion diffusion. To improve the reaction kinetics of Co_3O_4, Liu *et al.* prepared a Cu–Co-MOF by the coordination reaction between Cu-doped cobalt carbonate hydroxide (Cu-CCH) and 2-MIM, and oxygen vacancy-rich Cu–Co_3O_4 nanocrystals confined in carbon (O_v-Cu–Co_3O_4@C) were obtained after thermal treatment and reduction.[78] O_v-Cu–Co_3O_4@C showed significantly improved specific capacity and rate performance compared with Co_3O_4@C. Zhang *et al.* first used anodic electrodeposition to directly deposit a 2D layered Ni–Co-MOF on the surface of nickel foam.[79] Subsequent pyrolysis and activation led to the formation of a 2D carbon–metal oxide (CMO) composite electrode. The specific capacitance of 2D-CMO as a SC electrode was 2098 mF cm^{-2} at a current density of 1 mA cm^{-2}. After 4200 cycles in 4.0 M KOH solution, the specific capacitance remained at 92%. Kong *et al.* designed and fabricated ultrathin zinc–cobalt oxide nanosheet@N-doped carbon hollow nanowall arrays ($ZnCo_2O_4$@NC NWAs) from 2D Co-MOF arrays by a controlled cation exchange followed by two-step annealing.[80] The unique 3D self-supported nanostructures on flexible carbon fabrics (CTs) shortened the ion diffusion distance and enhanced the charge transfer, and the doping of Zn ions produced hollow structures as well as improved the electronic conductivity. Thus, the prepared $ZnCo_2O_4$@NC/CTs electrode showed a high specific capacitance of 2003.8 F g^{-1} at a current density of 1.8 A g^{-1}. Li and coworkers incorporated both Ni and Mn elements into a Co-MOF and prepared Co_3O_4/NiO/Mn_2O_3 nanosheets by a two-step annealing of the CoNiMn-MOF precursor.[81] Due to the synergistic effect of the three metals, the Co_3O_4/NiO/Mn_2O_3 nanosheet electrode provided a high specific capacitance of 3.65 mF cm^{-2} at a current density of 1 mA cm^{-2}. Acharya *et al.* prepared a hollow Zn–Ni–Co-oxide (ZNCO) nanosheet array on reduced graphene oxide modified nickel foam (rGO/NF), using a 2D bimetallic Zn–Co MOF as the template.[82] The prepared hierarchical ZNCO nanosheet array could afford a large number of active sites with short ion diffusion paths. As a binder-free electrode for SCs, it exhibited a specific capacity of 267 mA h g^{-1} at a current density of 1 A g^{-1} with an ultra-high rate capability (83.8% at 50 A g^{-1}). These MOF-derived metal oxide hollow materials have greatly improved electrochemical performance as electrode materials for SCs due to their unique compositional and structural advantages.

3.1.3 MOF-derived metal sulfides. Metal sulfides are of great interest as battery-type electrode materials for SCs because of their high theoretical capacity, multiple oxidation states for faradaic reactions and low cost. However, insufficient active sites and relative low electrical conductivity result in inferior rate capacity and poor cycling stability, which hinder the application of metal sulfides in practical energy storage. Rational design of self-supported porous nano-structures on conductive substrates with fully exposed active sites and good electronic conductivity is considered an effective way to boost the electrochemical properties of metal sulfides. MOFs have become important precursors for the preparation of porous metal sulfide nanoarrays due to their tunable structure, versatile morphology and high porosity.[83–86] For example, Han *et al.* first prepared porous cobalt sulfide nanosheet arrays on nickel foam (Co_9S_8–NSA/NF) by room-temperature deposition of a 2D leaf-like Co-based zeolite imidazole framework (Co-ZIF-L) on NF, followed by sulfidation with thioacetamide (TAA). The prepared Co_9S_8–NSA/NF was directly utilized as a binder-free electrode for SCs, which displayed a high specific capacitance (1098.8 F g^{-1} at a current density of 0.5 A g^{-1}) and good rate capability (54.6% retention at 10 A g^{-1}).[24] Compared to single-metal sulfides, mixed-metal sulfides exhibit higher electrochemical activity due to the enhanced charge transfer between different ions and the optimization of the electronic structure. In another work, Tao and co-workers have prepared bimetallic zinc–cobalt-based MOF (Zn/Co-MOF) nanosheets on NF by a simple co-assembly of Zn^{2+} and Co^{2+} with 2-MIM at room temperature.[87] Zn/Co-MOF was converted to Zn–Co–S/NF by hydrothermal sulfidation. Zn–Co–S/NF, as a freestanding SC electrode, exhibited excellent electrochemical activity (2354.3 F g^{-1} at 0.5 A g^{-1}), which outperformed the Zn–Co–S powdery electrode and CoS/NF due to the merits of bimetallic sulfide and the binder-free electrode. Le *et al.* prepared core–shell hollow iron–cobalt sulfide (Fe–Co–S) nanoarrays on conductive NF using Co-MOF as a sacrificial template (Fig. 6e).[73] $FeCo_2S_4$ nanosheet shells were assembled on Co_3S_4 hollow nanoarrays by finely manipulating the etching/ion exchange reaction between Co-MOF and $FeSO_4$ and subsequent solvothermal sulfidation to form hierarchical core–shell hollow nanostructures. LDH (Fig. 6f) was firstly generated on the Co-MOF surface during the ion etching/exchange process, and the hierarchical

structure was fully retained after sulfidation (Fig. 6g). The prepared Fe–Co–S/NF electrode had a specific capacitance of 2695 F g^{-1} at a current density of 1 A g^{-1}, and a capacitance retention of 84% after 1000 cycles. Zheng *et al.* developed a simple MOF engagement strategy to prepare nickel–cobalt–sulfide nanosheet arrays (Ni–Co–S) directly on NF and used them as binder-free electrodes for SCs.[88] With an ultra-high specific capacitance of 3724 F g^{-1}, they were superior to other bimetallic sulfides reported previously. Ternary metal sulfides exhibit superior electrochemical activity compared to bimetallic sulfides due to the synergy between different ions. For example, a novel mesoporous hollow Ni–Zn–Co–S nanosword array (NSA) was designed and synthesized from Zn–Co-ZIF by Huang *et al.*[89] The optimal Ni–Zn–Co–S-0.33 NSA electrode (Zn/Co = 1 : 2) exhibited a high areal capacity of 1.1 mA h cm^{-2}, corresponding to a high specific capacity of 358.1 mA h g^{-1} at a current density of 10 mA cm^{-2}, which was superior to bimetallic Ni–Co–S NSAs.

Diverse nanostructured electrode materials can be simply obtained by direct conversion of MOFs. The MOF derivative inherits the clear morphology of the parent MOF, retaining the open metal active sites and structural stability. It shows great potential in SCs. However, the single component electrode still cannot fulfill the requirements of high-performance SCs.

3.2 MOF derivatives as the scaffolds for anchoring secondary electrode materials

Metal oxides and metal sulfides, which have the advantages of low cost, high natural abundance and high theoretical capacity, are the most used faradaic electrode materials. However, the use of single metal oxide or metal sulfide nanoparticles as electrode materials still faces some inherent problems such as insufficient redox reactive sites, low electrical conductivity and poor cycling stability. Various feasible strategies have been proposed to address these obstacles. For example, some researchers have used MOF derivatives as a scaffold for anchoring secondary electrode materials to synthesize core–shell nanostructured materials with multiple functions to enhance the electrochemical performance. These core–shell nanostructures including nanospheres, nanoprisms and nanocubes can provide high active surface areas and short diffusion paths for ions and electrons. However, the fragile structure of the shell materials and the easy aggregation of the core limited their application as SC electrode materials.[90–93] Growing self-supported nanoarrays of core–shell structured materials on conducting substrates is considered to be an effective strategy to address this challenge. For example, Han *et al.* firstly synthesized Co-MOF nanosheets on carbon cloth (CC) substrates by a solution method at room temperature. Next, Co_3O_4 nanosheets were obtained by calcining the Co-MOF template under an air atmosphere. Finally, Co_3O_4 nanosheets were used as a backbone to prepare the final petal-like CC/Co_3O_4@$CoNi_2S_4$ nanosheet arrays by an electrodeposition process (Fig. 7a).[94] The electrode showed a specific capacity of 244.4 mA h g^{-1} at a current density of 1 A g^{-1} and an excellent rate capability of 81.3% at a current density of 16 A g^{-1}. Tao *et al.* constructed a novel $NiCo_2O_4$ nanosheet decorated Co_3O_4 nanoarray on NF by using a leaf-like Co-MOF as a template (Fig. 7b).[95] As a binder-free electrode for SCs, it displayed a specific capacity of 544.2 C g^{-1} at a current density of 1 A g^{-1}, which was 9.3 times higher than that of the Co_3O_4 or $NiCo_2O_4$ electrode, demonstrating the advantages of self-supported core–shell nanoarrays. Sun *et al.* used a simple solution method to grow homogeneous Zn/Co-MOF nanosheet arrays directly on CC substrates.[96] Subsequently, ZnCoS nanosheet arrays were obtained by calcination and a hydrothermal anion exchange reaction, and it was used as a scaffold for the deposition of $Ni(OH)_2$ and VN, respectively. $Ni(OH)_2$@ZnCoS and VN@ZnCoS were assembled into an ASC device, which exhibited an ultra-high energy density (75 W h kg^{-1} at a power density of 0.4 kW kg^{-1}) and excellent cycling stability (a capacitance retention rate of 92% after 10 000 cycles).

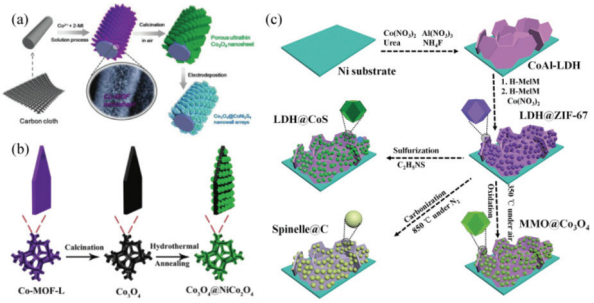

Fig. 7 (a) Schematic illustrating the synthesis procedure of CC/Co_3O_4@$CoNi_2S_4$. Reprinted with permission from ref. 94, Copyright 2020, Royal Society of Chemistry. (b) Schematic illustration of the fabrication of Co_3O_4@$NiCo_2O_4$ nanoarrays. Reprinted with permission from ref. 95, Copyright 2019, Royal Society of Chemistry. (c) Schematic illustration of the fabrication of hierarchically structured MMO@Co_3O_4, spinelle@C and LDH@CoS derived from CoAl-LDH@ZIF-67. Reprinted with permission from ref. 97, Copyright 2016, Royal Society of Chemistry.

The above results indicate that the combination of MOF-derived core–shell structured nanomaterials and conducting substrates can improve the electrochemical performance of single component electrode materials. This strategy can be adopted to construct various core–shell nanoarrays on conductive substrates. However, to achieve a synergetic effect of different electrode materials, the type of electrode materials, growth sequence and template morphology should be taken into full consideration for a better understanding of the assembly of the core–shell structure.

3.3 Decorating MOF derivatives on micro-/nanoarrays

The elaborate design and fabrication of hierarchically integrated electrodes by anchoring MOF derivatives on highly conductive active materials have attracted increasing interest in recent years. This will compensate for the inherent defects of the MOF derivatives, giving rise to improved specific capacitance and cycling stability. For example, Dou *et al.* prepared CoAl-LDH@ZIF-67 by the *in situ* growth of ZIF-67 on CoAl-LDH

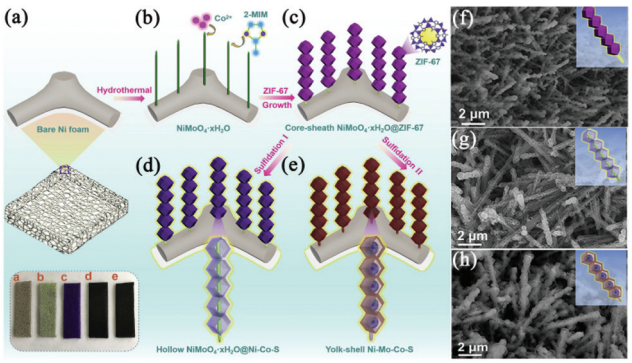

Fig. 8 (a–e) Schematic illustrations of the synthesis of yolk–shell Ni–Mo–Co–S NCAs on NF. SEM images of (f) $NiMoO_4{\cdot}xH_2O$@ZIF-67, (g) hollow $NiMoO_4{\cdot}xH_2O$@Ni–Co–S NCAs and (h) yolk–shell Ni–Mo–Co–S NCAs. Reprinted with permission from ref. 98, Copyright 2020, Elsevier.

nanoflakes fabricated on NF.[97] Subsequently, LDH@ZIF-67 was utilized as a template/precursor to obtain mixed metal oxides (MMO)@Co_3O_4, spinelle@C and LDH@CoS by oxidization, carbonization and sulfidation, respectively (Fig. 7c). The resulting hierarchical derivatives showed enhanced electrochemical properties due to the strong electronic coupling of heterostructures and the synergistic effect between different components. Fei *et al.* designed and synthesized sugarloaf-like multicomponent yolk–shell Ni–Mo–Co–S nanocage arrays (NCAs) on NF by a simple MOF engagement strategy (Fig. 8a–e).[98] ZIF-67 nanocrystals were first deposited on $NiMoO_4{\cdot}xH_2O$ nanorods to form core–sheath $NiMoO_4{\cdot}xH_2O$@ZIF-67, and $NiMoO_4{\cdot}xH_2O$@ZIF-67 was transformed into hollow $NiMoO_4{\cdot}xH_2O$@Ni–Co–S NCAs (Fig. 8g) and yolk–shell Ni–Mo–Co–S NCAs (Fig. 8h) after sulfidation with low and large dosages of TAA, respectively. Benefiting from the interesting structural and compositional advantages, the yolk–shell NiMoCo–S NCAS/NF binderless electrode exhibited an extremely high area capacity of 1.96 mA h cm^{-2} at a current density of 5 mA cm^{-2}. Dai *et al.* prepared a hollow S-doped Co_3O_4 sheath on CoO nanowires by a two-step synthesis including the surface etching of CoO nanowires for the simultaneous *in situ* growth of well-aligned ZIF-67 and subsequent sulfidation.[99] The synergistic effect between conductive CC and the hollow ordered nanoarrays ensured efficient mass and electron transport. Thus, the core–shell nanoarrays displayed a high areal capacitance of 1.013 F cm^{-2} at 1 mA cm^{-2}. Tang *et al.* perfectly decorated MOF-derived $Zn_{0.76}Co_{0.24}S$ nanoparticle@C on $Zn_{0.76}Co_{0.24}S$ nanosheet arrays ($Zn_{0.76}Co_{0.24}S$ CSNSAs).[100] As a free-standing electrode material for SCs, it provided a high specific capacity of 1202 C g^{-1} at a current density of 1 A g^{-1}.

Anchoring MOF derivatives on highly conductive active materials can significantly improve the electronic conductivity of electrodes. Besides, the hierarchical structure provides a large specific surface area and also prevents the aggregation of MOF derivatives. Thus, boosted electrochemical performance is realized.

4 Conclusions and perspectives

This review summarizes the recent advances in self-supported MOF-based nanostructures including pristine MOFs, MOF composites and MOF derivative arrays as binder-free electrodes for SCs, and the synthesis strategy of these nanostructures is overviewed. The advantages of self-supported MOF-based nanostructures as electrodes for SCs, such as a simplified electrode preparation process, enhanced electronic conductivity and largely exposed electroactive sites are highlighted. However, there are still a number of issues and challenges need to be addressed for practical applications. First, in order to produce practical devices, the mass loading of the electroactive materials on a current collector needs to exceed 10 mg cm^{-2}. However, many self-supported MOF-based electrodes have a mass loading of only a few tens to hundreds of micrograms, and the electroactive materials are not uniformly distributed. Second, although MOF-based nanostructures show high specific capacitance in three-electrode systems, the assembled two-electrode cell usually displays moderate energy storage properties due to the mismatching electrochemical performance between the positive and negative electrodes. In this regard, energy storage devices with both electrodes using self-supported MOF-based nanostructures derived from one single precursor are more advantageous, since the two electrodes share similar properties. Moreover, the assembly of the devices should be intensively studied and optimized. Finally, the choice of MOF precursors for self-supported electrodes is mainly limited to a few MOFs, which means that the application potential of other MOFs has not yet been explored. Therefore, great works from MOF crystal design to electrode preparation and device assembly are needed to obtain the desirable electrochemical performance. Impressively, MOF-templated hierarchical core–shell nanoarrays have recently attracted much attention. In such core–shell nanostructures, the disadvantages of individual components are compensated and a synergetic effect between different components is realized. This strategy offers an opportunity to manipulate the overall performance of electrode materials.

In conclusion, self-supported MOF-based nanostructures with exciting energy storage properties have emerged as new generation binder-free electrodes for SCs. We hope that this review can provide an overview on this highly exciting field, and will stimulate more explorations on this topic promoting the application of MOF-based electrode materials in high-performance electrochemical energy storage devices.

Author contributions

Xueyan Zhao: writing – the original draft. Kai Tao: conceptualization, supervision and writing – review and editing. Lei Han: supervision and writing – review and editing.

Conflicts of interest

There are no conflicts to declare.

Acknowledgements

This work was financially supported by the Zhejiang Provincial Natural Science Foundation of China (LY20E020005) and the National Science Foundation of China (5157227 and 221971131).

References

1 K. Zhang, K. O. Kirlikovali, L. Quyet Van, Z. Jin, R. S. Varma, H. W. Jang, O. K. Farha and M. Shokouhimehr, *ACS Appl. Nano Mater.*, 2020, **3**, 3964–3990.
2 S. Tajik, H. Beitollahi, F. G. Nejad, K. O. Kirlikovali, L. Quyet Van, H. W. Jang, R. S. Varma, O. K. Farha and M. Shokouhimehr, *Cryst. Growth Des.*, 2020, **20**, 7034–7064.
3 A. E. Baumann, D. A. Burns, B. Liu and V. S. Thoi, *Commun. Chem.*, 2019, **2**, 86.
4 H. B. Wu and X. W. D. Lou, *Sci. Adv.*, 2017, **3**, eaap9252.
5 S. Liu, L. Kang, J. Zhang, S. C. Jun and Y. Yamauchi, *ACS Energy Lett.*, 2021, **6**, 4127–4154.
6 S. Liu, L. Kang, J. Henzie, J. Zhang, J. Ha, M. A. Amin, M. S. A. Hossain, S. C. Jun and Y. Yamauchi, *ACS Nano*, 2021, **15**, 18931–18973.
7 J. Liao, C. Chen, Q. Hu, Y. Du, Y. He, Y. Xu, Z. Zhang and X. Zhou, *Angew. Chem., Int. Ed.*, 2021, **60**, 25575–25582.
8 Y. Du, Z. Yi, B. Chen, J. Xu, Z. Zhang, J. Bao and X. Zhou, *J. Energy Chem.*, 2022, **66**, 413–421.
9 X. Xu, L. Si, X. Zhou, F. Tu, X. Zhu and J. Bao, *J. Power Sources*, 2017, **349**, 37–44.
10 R. R. Salunkhe, Y. V. Kaneti and Y. Yamauchi, *ACS Nano*, 2017, **11**, 5293–5308.
11 Q. Yang, *Acta Phys. Chim. Sin.*, 2020, **36**, 1910030.
12 H. Zhao, L. Liu, R. Vellacheri and Y. Lei, *Adv. Sci.*, 2017, **4**, 1700188.
13 D. Sheberla, J. C. Bachman, J. S. Elias, C.-J. Sun, Y. Shao-Horn and M. Dinca, *Nat. Mater.*, 2017, **16**, 220–224.
14 W. Xia, A. Mahmood, R. Q. Zou and Q. Xu, *Energy Environ. Sci.*, 2015, **8**, 1837–1866.
15 X. Y. Zhao, Q. X. Ma, K. Tao and L. Han, *ACS Appl. Energy Mater.*, 2021, **4**, 4199–4207.
16 A. Saad, S. Biswas, E. Gkaniatsou, C. Sicard, E. Dumas, N. Menguy and N. Steunou, *Chem. Mater.*, 2021, **33**, 5825–5849.
17 S. Dang, Q.-L. Zhu and Q. Xu, *Nat. Rev. Mater.*, 2018, **3**, 17075.
18 L. Meng, B. Yu and Y. Qin, *Commun. Chem.*, 2021, **4**, 82.
19 H. B. Zhang, J. W. Nai, L. Yu and X. W. Lou, *Joule*, 2017, **1**, 77–107.
20 B. Y. Guan, X. Y. Yu, H. B. Wu and X. W. Lou, *Adv. Mater.*, 2017, **29**, 1703614.
21 T. Yue, C. Xia, X. Liu, Z. Wang, K. Qi and B. Y. Xia, *ChemElectroChem*, 2021, **8**, 1021–1034.
22 J. Wang, Q. Zhong, Y. Q. Zeng, D. Y. Cheng, Y. H. Xiong and Y. F. Bu, *J. Colloid Interface Sci.*, 2019, **555**, 42–52.
23 Y. Liu, N. Xin, Q. Yang and W. Shi, *J. Colloid Interface Sci.*, 2021, **583**, 288–298.
24 X. Han, K. Tao, D. Wang and L. Han, *Nanoscale*, 2018, **10**, 2735–2741.
25 L. Feng, X. Han, X. R. Su, B. C. Pang, Y. L. Luo, F. Hu, M. J. Zhou, K. Tao and Y. Y. Xia, *J. Alloys Compd.*, 2018, **765**, 512–519.
26 B. Singh and A. Indra, *Chem. – Asian J.*, 2020, **15**, 607–623.
27 G. Cai, W. Zhang, L. Jiao, S.-H. Yu and H.-L. Jiang, *Chem*, 2017, **2**, 791–802.
28 H. Liang, A. Yao, X. Jiao, C. Li and D. Chen, *ACS Appl. Mater. Interfaces*, 2018, **10**, 20396–20403.
29 Y. Wang, A. Wang, Z. Xue, L. Wang, X. Li and G. Wang, *J. Mater. Chem. A*, 2021, **9**, 22597–22602.
30 B. Singh, A. Singh, A. Yadav and A. Indra, *Coord. Chem. Rev.*, 2021, **447**, 214144.
31 L. Wan and P. Wang, *Int. J. Hydrogen Energy*, 2021, **46**, 8356–8376.
32 Q. Cheng, K. Tao, X. Han, Y. Yang, Z. Yang, Q. Ma and L. Han, *Dalton Trans.*, 2019, **48**, 4119–4123.
33 W. W. Li, X. Y. Zhao, Q. Bi, Q. X. Ma, L. Han and K. Tao, *Dalton Trans.*, 2021, **50**, 11701–11710.
34 Y. Xue, G. Zhao, R. Yang, F. Chu, J. Chen, L. Wang and X. Huang, *Nanoscale*, 2021, **13**, 3911–3936.
35 A. Dhakshinamoorthy, A. M. Asiri and H. Garcia, *Adv. Mater.*, 2019, **31**, 1900617.
36 Y. Xu, Q. Li, H. Xue and H. Pang, *Coord. Chem. Rev.*, 2018, **376**, 292–318.
37 Y. Xue, S. Zheng, H. Xue and H. Pang, *J. Mater. Chem. A*, 2019, **7**, 7301–7327.
38 W. Liu, R. Yin, X. Xu, L. Zhang, W. Shi and X. Cao, *Adv. Sci.*, 2019, **6**, 1802373.
39 W. Xia, A. Mahmood, R. Zou and Q. Xu, *Energy Environ. Sci.*, 2015, **8**, 1837–1866.
40 W.-H. Li, K. Ding, H.-R. Tian, M.-S. Yao, B. Nath, W.-H. Deng, Y. Wang and G. Xu, *Adv. Funct. Mater.*, 2017, **27**, 1702067.
41 M. Zhao, Q. Lu, Q. Ma and H. Zhang, *Small Methods*, 2017, **1**, 1600030.
42 G. Chakraborty, I.-H. Park, R. Medishetty and J. J. Vittal, *Chem. Rev.*, 2021, **121**, 3751–3891.
43 L. Yao, J. Lin, H. Yang, Q. Wu, D. Wang, X. Li, L. Deng and Z. Zheng, *Nanoscale*, 2019, **11**, 11086–11092.
44 J. Ma, J. Li, R. Guo, H. Xu, F. Shi, L. Dang, Z. Liu, J. Sun and Z. Lei, *J. Power Sources*, 2019, **428**, 124–130.
45 F. Zhang, J. L. Zhang, J. J. Ma, X. Y. Zhao, Y. Y. Li and R. Q. Li, *J. Colloid Interface Sci.*, 2021, **593**, 32–40.
46 J. Yang, P. Xiong, C. Zheng, H. Qiu and M. Wei, *J. Mater. Chem. A*, 2014, **2**, 16640–16644.
47 N. Raza, T. Kumar, V. Singh and K.-H. Kim, *Coord. Chem. Rev.*, 2021, **430**, 213660.

48 J. Wang, Q. Zhong, Y. Zeng, D. Cheng, Y. Xiong and Y. Bu, *J. Colloid Interface Sci.*, 2019, **555**, 42–52.
49 F. Ren, Y. Ji, F. Chen, Y. Qian, J. Tian and J. Wang, *Mater. Chem. Front.*, 2021, **5**, 7333–7342.
50 Y. Chen, N. Wang, W. Hu and S. Komarneni, *J. Porous Mater.*, 2019, **26**, 921–929.
51 T. Deng, Y. Lu, W. Zhang, M. Sui, X. Shi, D. Wang and W. Zheng, *Adv. Energy Mater.*, 2018, **8**, 1702294.
52 J. Zhang, Z. Wang, T. Deng and W. Zhang, *Nanotechnology*, 2021, **32**, 195404.
53 S. Xu, R. Liu, X. Shi, Y. Ma, M. Hong, X. Chen, T. Wang, F. Li, N. Hu and Z. Yang, *Electrochim. Acta*, 2020, **342**, 136124.
54 X. M. Cao and Z. B. Han, *Chem. Commun.*, 2019, **55**, 1746–1749.
55 B. Chen, L. Xu, Z. Xie and W.-Y. Wong, *EcoMat*, 2021, **3**, e12106.
56 T. Li, Y. Bai, Y. Wang, H. Xu and H. Jin, *Coord. Chem. Rev.*, 2020, **410**, 213221.
57 Q. Bi, Q. Ma, K. Tao and L. Han, *Dalton Trans.*, 2021, **50**, 8179–8188.
58 G. Li, H. R. Cai, X. L. Li, J. Zhang, D. S. Zhang, Y. F. Yang and J. Xiong, *ACS Appl. Mater. Interfaces*, 2019, **11**, 37675–37684.
59 F. Yang, H. Guo, Y. Chen, M. Xu, W. Yang, M. Wang, M. Yang, J. Zhang, L. Sun, T. Zhang and W. Yang, *Chem. – Eur. J.*, 2021, **27**, 14478–14488.
60 X. Hu, S. Liu, Y. Wang, X. Huang, J. Jiang, H. Cong, H. Lin and S. Han, *J. Colloid Interface Sci.*, 2021, **600**, 72–82.
61 X.-M. Cao and Z.-B. Han, *Chem. Commun.*, 2019, **55**, 1746–1749.
62 Y. V. Kaneti, S. Dutta, M. S. A. Hossain, M. J. A. Shiddiky, K. L. Tung, F. K. Shieh, C. K. Tsung, K. C. W. Wu and Y. Yamauchi, *Adv. Mater.*, 2017, **29**, 1700213.
63 C. Young, J. Wang, J. Kim, Y. Sugahara, J. Henzie and Y. Yamauchi, *Chem. Mater.*, 2018, **30**, 3379–3386.
64 Y.-N. Liu, H.-T. Wang, X.-H. Kang, Y.-F. Wang, S.-Y. Yang and S.-W. Bian, *J. Power Sources*, 2018, **402**, 413–421.
65 B. Liu, H. Shioyama, T. Akita and Q. Xu, *J. Am. Chem. Soc.*, 2008, **130**, 5390–5391.
66 Y. V. Kaneti, J. Tang, R. R. Salunkhe, X. Jiang, A. Yu, K. C. Wu and Y. Yamauchi, *Adv. Mater.*, 2017, **29**, 1604898.
67 M. H. Yap, K. L. Fow and G. Z. Chen, *Green Energy Environ.*, 2017, **2**, 218–245.
68 X. Cao, C. Tan, M. Sindoro and H. Zhang, *Chem. Soc. Rev.*, 2017, **46**, 2660–2677.
69 Y. Liu, G. Li, Y. Guo, Y. Ying and X. Peng, *ACS Appl. Mater. Interfaces*, 2017, **9**, 14043–14050.
70 J. Zhang, W. Li, T. Ahmed Shifa, J. Sun, C. Jia, Y. Zhao and Y. Cui, *J. Power Sources*, 2019, **439**, 227066.
71 Y. Song, M. Zhang, T. Liu, T. Li, D. Guo and X.-X. Liu, *Nanomaterials*, 2019, **9**, 1110.
72 C. Zhang, J. Xiao, X. Lv, L. Qian, S. Yuan, S. Wang and P. Lei, *J. Mater. Chem. A*, 2016, **4**, 16516–16523.
73 K. Le, M. Gao, W. Liu, J. Liu, Z. Wang, F. Wang, V. Murugadoss, S. Wu, T. Ding and Z. Guo, *Electrochim. Acta*, 2019, **323**, 134826.
74 S. Wu, J. Liu, H. Wang and H. Yan, *Int. J. Energy Res.*, 2019, **43**, 697–716.
75 X.-C. Xie, K.-J. Huang and X. Wu, *J. Mater. Chem. A*, 2018, **6**, 6754–6771.
76 Y. Li, Y. Xu, W. Yang, W. Shen, H. Xue and H. Pang, *Small*, 2018, **14**, 1704435.
77 S. Liu, L. Kang, J. Zhang, E. Jung, S. Lee and S. C. Jun, *Energy Storage Mater.*, 2020, **32**, 167–177.
78 S. Liu, L. Kang, J. Hu, E. Jung, J. Zhang, S. C. Jun and Y. Yamauchi, *ACS Energy Lett.*, 2021, **6**, 3011–3019.
79 X. Zhang, J. Luo, P. Tang, X. Ye, X. Peng, H. Tang, S.-G. Sun and J. Fransaer, *Nano Energy*, 2017, **31**, 311–321.
80 D. Kong, Y. Wang, S. Huang, J. Hu, Y. V. Lim, B. Liu, S. Fan, Y. Shi and H. Y. Yang, *Energy Storage Mater.*, 2019, **23**, 653–663.
81 S. Li, Y. Duan, Y. Teng, N. Fan and Y. Huo, *Appl. Surf. Sci.*, 2019, **478**, 247–254.
82 J. Acharya, B. Pant, G. P. Ojha, H. S. Kong and M. Park, *J. Colloid Interface Sci.*, 2021, **602**, 573–589.
83 W. Zhan, L. Sun and X. Han, *Nano–Micro Lett.*, 2019, **11**, 1.
84 J. M. Gonçalves, P. R. Martins, D. P. Rocha, T. A. Matias, M. S. S. Julião, R. A. A. Munoz and L. Angnes, *J. Mater. Chem. C*, 2021, **9**, 8718–8745.
85 T. Chen, X. Liu, L. Niu, Y. Gong, C. Li, S. Xu and L. Pan, *Inorg. Chem. Front.*, 2020, **7**, 567–582.
86 J. Ma, W. Li, X. Zhang, Y. Cheng and F. Zhang, *Appl. Surf. Sci.*, 2020, **507**, 145074.
87 K. Tao, X. Han, Q. Cheng, Y. Yang, Z. Yang, Q. Ma and L. Han, *Chem. – Eur. J.*, 2018, **24**, 12584–12591.
88 L. Zheng, J. Song, X. Ye, Y. Wang, X. Shi and H. Zheng, *Nanoscale*, 2020, **12**, 13811–13821.
89 Y. Huang, L. Quan, T. Liu, Q. Chen, D. Cai and H. Zhan, *Nanoscale*, 2018, **10**, 14171–14181.
90 K.-C. Ho and L.-Y. Lin, *J. Mater. Chem. A*, 2019, **7**, 3516–3530.
91 H. P. Feng, L. Tang, G. M. Zeng, Y. Zhou, Y. C. Deng, X. Ren, B. Song, C. Liang, M. Y. Wei and J. F. Yu, *Adv. Colloid Interface Sci.*, 2019, **267**, 26–46.
92 L.-b. Jiang, X.-z. Yuan, J. Liang, J. Zhang, H. Wang and G.-m. Zeng, *J. Power Sources*, 2016, **331**, 408–425.
93 B. Zhang, F. Kang, J.-M. Tarascon and J.-K. Kim, *Prog. Mater. Sci.*, 2016, **76**, 319–380.
94 D. Han, J. Wei, Y. Zhao, Y. Shen, Y. Pan, Y. Wei and L. Mao, *Inorg. Chem. Front.*, 2020, **7**, 1428–1436.
95 K. Tao, Y. Yang, C. Yang, Q. Ma and L. Han, *Dalton Trans.*, 2019, **48**, 14156–14163.
96 W. Sun, Y. Du, G. Wu, G. Gao, H. Zhu, J. Shen, K. Zhang and G. Cao, *J. Mater. Chem. A*, 2019, **7**, 7138–7150.
97 Y. Dou, J. Zhou, F. Yang, M.-J. Zhao, Z. Nie and J.-R. Li, *J. Mater. Chem. A*, 2016, **4**, 12526–12534.
98 B. Fei, Z. Yao, D. Cai, J. Si, Q. Wang, Q. Chen, B. Sa, K. Peng and H. Zhan, *Energy Storage Mater.*, 2020, **25**, 105–113.
99 S. Dai, Y. Yuan, J. Yu, J. Tang, J. Zhou and W. Tang, *Nanoscale*, 2018, **10**, 15454–15461.
100 Q. Tang, L. Ma, F. Yan, M. Gan, X. Li, F. Cao, M. Ye, Y. Zhai and Y. Zhou, *Synth. Met.*, 2019, **250**, 136–145.

